

Astro Generative Network: A Variational Framework for Controlled Node Insertion in Incomplete Complex Networks

Mehrdad Jalali^{1,4}, Binh Vu^{1,2}, Swati Chandna¹ and Chen Ding³

¹*Applied Data Science and Artificial Intelligence, SRH University Heidelberg, Heidelberg, Germany*

²*Faculty of Mathematics and Computer Science, FernUniversität in Hagen, Hagen, Germany*

³*Department of Computer Science, Toronto Metropolitan University, Toronto, Canada*

⁴*Corresponding author: mehrdad.jalali@srh.de*

Abstract

Empirical networked systems are often *partially observed*: sampling frames, crawling policies, privacy constraints, and temporal gaps yield graphs with missing actors and edges. Such incompleteness complicates robustness and sensitivity analyses because many graph-learning pipelines implicitly treat the observed node set as exhaustive. Link prediction and graph completion typically repair structure among *known* vertices; full-graph generators synthesize new graphs but do not treat an observed network as a fixed backbone to extend. We target the complementary task of *controlled node insertion*: generating plausible new actors and attaching them to an existing graph so that global topology remains interpretable.

We present the Astro Generative Network (AGN), a variational graph autoencoder (VGAE) that samples latent vectors to decode node features, then integrates new vertices with similarity-based attachment to the original backbone. We distinguish the recommended configuration (no edges among generated nodes) from AGN-original (a diagnostic baseline that allows generated-generated edges). Across three synthetic regimes—community-structured, multi-community, and scale-free sparse graphs—AGN-original produces dense generated-generated subgraphs that inflate clustering and density; disabling those edges removes the artifact while preserving degree and path-length behavior. Under AGN, clustering changes lie within about $\pm 5.4\%$ and modularity within about $\pm 16.9\%$ relative to pre-insertion values in our experiments; distributional novelty metrics indicate non-trivial separation from existing nodes without claiming domain-grounded identities.

The contribution is methodological: a reproducible insertion protocol and evaluation lens for incomplete network science and engineering, supporting what-if analyses of missing actors, integration diagnostics, and topology-aware augmentation without replacing link prediction, full-graph generation, or temporal evolution models.

Keywords: Incomplete networks; partially observed graphs; controlled node insertion; network augmentation; variational graph autoencoder; topology preservation; network robustness.

1 Introduction

Empirical social and engineered networks are rarely complete. Surveys and platforms observe subsets of actors; crawlers follow biased link trajectories; administrative records omit participants; and longitudinal snapshots miss arrivals between waves. From a network science and engineering (NSE) perspective, the practical question is not only “which edges are missing among those we see?” but also “how sensitive are our descriptors and algorithms if additional actors plausibly belong to the system?” Metrics such as clustering, modularity, and path length can shift when

vertices are absent or when augmentation is performed carelessly; understanding that sensitivity supports more honest reporting under partial observation.

Most graph-learning tools assume a *fixed* vertex set at inference: link prediction and graph completion score candidate edges among existing nodes [3]; generative models often synthesize *entire* graphs from scratch [1, 2, 6]. Dynamic and temporal models forecast trajectories for *known* identities rather than supplying a controlled procedure for inserting hypothetical new actors into a fixed observed backbone. None of these lines of work is wrong for its own target task; the gap is the absence of a standardized, topology-aware protocol for *controlled node insertion*—adding vertices whose features are generated under a learned model while keeping the original graph as the structural reference.

We use *controlled* to emphasize explicit policies for (i) how many nodes to add, (ii) how they attach to the existing graph, and (iii) which edge types are permitted. *Structural compatibility* means that post-insertion statistics remain interpretable relative to the pre-insertion graph; *novelty* means generated feature vectors are not trivial copies of observed rows. The tension between the two is central: memorization yields negligible novelty, whereas unconstrained wiring can distort global topology.

This work introduces the Astro Generative Network (AGN), a VGAE-based pipeline for controlled insertion. A graph convolutional encoder and Gaussian latent model capture regularities of the observed graph; new latent vectors are sampled from the prior and decoded into feature vectors; vertices are then attached to the top- k most similar *original* nodes subject to a cosine threshold. We distinguish **AGN**, the recommended configuration with *no* edges between generated nodes, from **AGN-original**, which allows generated-generated edges and serves only as a diagnostic baseline. Our experiments show that AGN-original can allocate most new edges within the generated set, producing an artificial dense patch that masquerades as “strong” integration on scalar metrics; AGN removes that failure mode by construction.

AGN is complementary to structure-preserving *reduction* under a fixed vertex universe, as in graph sparsification methods such as the Black Hole Strategy [25]: reduction compresses an observed graph for efficiency, whereas AGN expands it for counterfactual and robustness-style analyses. Both seek controlled transformations that preserve interpretable topology, but operate in opposite directions.

Fig. 1 summarizes the pipeline (astrophysical metaphor for intuition only; all mechanisms are graph-theoretic).

The main contributions of this work are as follows:

1. **Problem framing for NSE.** We articulate controlled node insertion as distinct from link prediction, full-graph generation, graph completion among fixed vertices, and temporal network models, with emphasis on partially observed systems and backbone preservation.
2. **Method.** We present AGN—VGAE-based feature generation with similarity-based attachment—and an explicit generated-generated edge policy, contrasting recommended AGN with diagnostic AGN-original.
3. **Evidence and diagnostics.** On three synthetic topologies, we report topology preservation, distributional novelty, baselines, and task-level checks, with edge-composition diagnostics that distinguish genuine integration from generated-only dense subgraphs.
4. **Limitations.** We discuss sparsity, modularity interpretation, hand-crafted features, and mixed ablations so that scope remains aligned with the reported experiments.

2 Related Work

This section is a guided map for readers coming from either network science or graph ML. For each family, we summarize its core objective, strengths, and the remaining gap for controlled

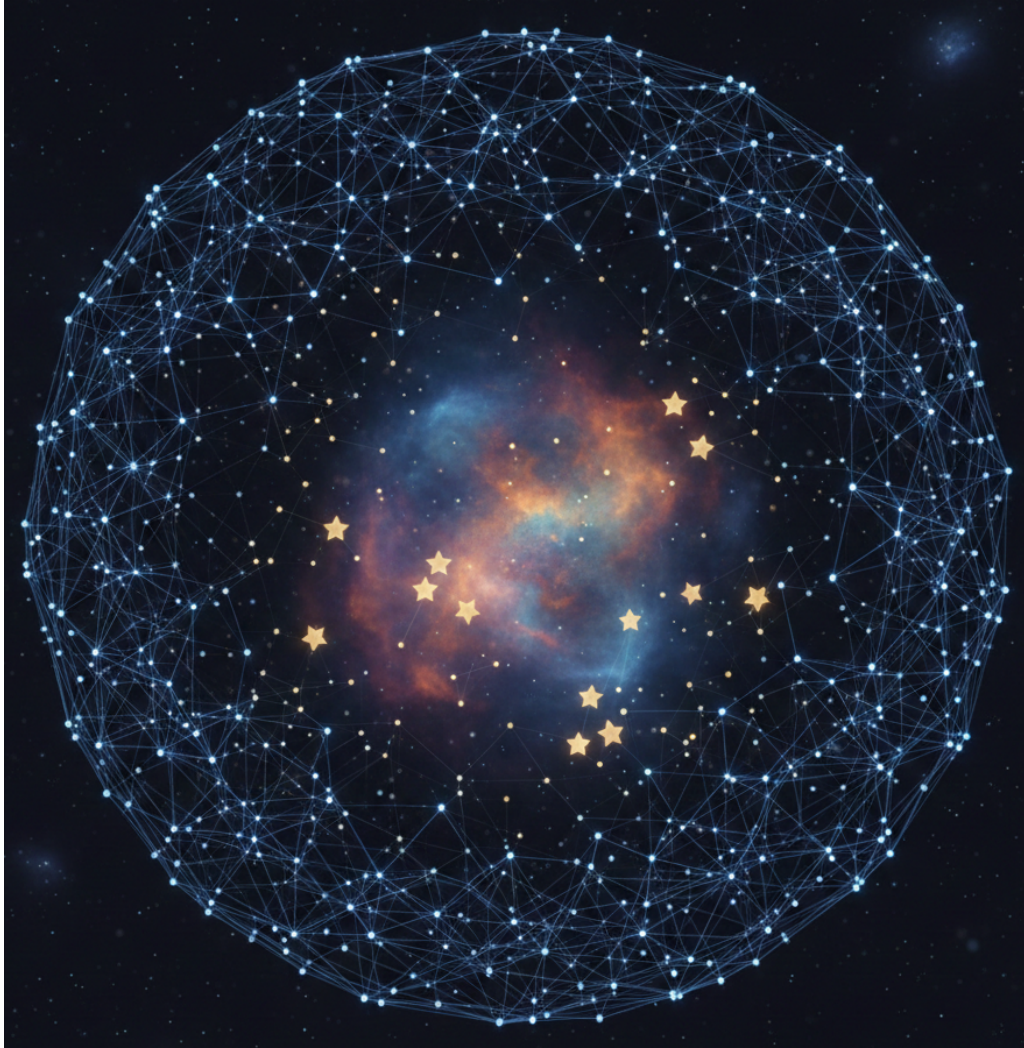


Figure 1: Conceptual illustration of controlled insertion: new vertices are proposed in latent space and integrated into the observed graph via similarity-based attachment. The figure is metaphorical; AGN does not use physical dynamics.

insertion into a *fixed* observed backbone. Table 1 gives a one-glance comparison; Sec. 2.8 distills takeaways.

2.1 Incomplete Networks, Partially Observed Graphs, and Missing Actors

Networked systems in engineering and the social sciences are observed through measurement pipelines: samples cover subpopulations, platforms hide edges, and crawlers introduce traversal bias [28–30]. As a result, many summary statistics can depend on whether unobserved actors would have bridged communities or altered cores; missingness over actors and ties can induce systematic measurement bias [31]. Controlled node insertion provides a transparent stress test: insert hypothetical vertices under explicit generation and attachment rules, then measure structural sensitivity. The goal is counterfactual analysis, not recovery of ground truth identities. An analogous bias concern appears in engineering topology measurement, where path-based sampling can distort inferred degree structure [32].

2.2 Variational Graph Autoencoders and Attributed Graph Modeling

Variational Graph Autoencoders (VGAEs) [3] extend variational autoencoders [2] to attributed graphs: GCN encoders [4] map vertices to Gaussian latent factors, and an inner-product decoder scores edges via $p(A_{ij} = 1 | \mathbf{z}_i, \mathbf{z}_j) = \sigma(\mathbf{z}_i^\top \mathbf{z}_j)$. Variants such as ARGA/ARVGA [16] and SIG-VAE [17] improve latent regularity or expressiveness for link prediction and clustering. GraphVAE [6] and conditional VGAEs [19] target *whole-graph* sampling. These lines excel at representation learning and at scoring or generating edges *among vertices that the model already indexes*. They do not, by themselves, specify a policy for introducing new vertex identities into a held-out backbone graph while reporting integration quality—that is the insertion layer AGN adds downstream of a VGAE backbone.

2.3 Graph Generation versus Graph Augmentation

Generation conventionally means sampling a new graph instance; *augmentation* can mean enriching training signals for a fixed vertex set. VGAE-related work has been used for molecular and social graph generation by decoding full adjacency structure from latent draws, typically assuming a closed vertex index set during training. Augmentation pipelines often create contrastive views or perturbed features: semi-implicit graph VAEs [17] and structured variational feature decoders [18] improve representations or impute attributes on the *same* vertices. Topological augmentation for GNNs [20] enriches signals via higher-order constructs but still centers on improving models over a given graph. These are valuable when the vertex set is fixed; they do not replace an explicit protocol for expanding V with new elements and measuring how the augmented graph relates to the original.

2.4 Node Insertion versus Graph Completion and Link Prediction

Link prediction and graph completion [3] rank or classify missing edges among *known* endpoints—interpolation within a fixed V . Classical growth models such as preferential attachment [9] explain scaling in *generative* network formation but are not likelihood-based fits to an observed empirical graph. Community-oriented generative proposals [21] synthesize new community layouts as full graphs rather than attaching hypothetical actors to a specific observed G . Controlled insertion sits between these poles: it requires new vertex feature vectors and a wiring rule that references the existing backbone, so evaluation must track both global topology relative to G and local statistics of how new edges split between original and generated endpoints.

2.5 Dynamic Graph Growth and Temporal Models

Temporal and dynamic graph models forecast events—edge creation, deletion, or weight change—along a timeline, usually conditioning on a known identity set at each step. Their strength is ordered evolution and short-horizon prediction under observed dynamics, and related graph generators can model sequential or iterative dynamics [5, 24]. AGN addresses a different question: “what if additional actors were present in this observed snapshot?” That counterfactual requires explicit insertion rules under partial observation, so AGN is positioned as a *static-snapshot* augmentation method that is complementary to temporal modeling.

2.6 Alternative Graph Generative Paradigms: GANs, Autoregressive Models, and Diffusion

GAN-based graph learning (e.g., GraphGAN, NetGAN [7, 8]) and autoregressive generators such as GraphRNN [5] have advanced the realism of synthetic graphs. Diffusion models for graphs [22, 23] and VGAE–diffusion hybrids [24] improve sample quality for full-graph generation. These families are strong when the target is a distribution over entire graphs or walks. For

insertion, however, one needs a *conditional* contract with the observed G : which edges are immutable, which vertices are new, and how to detect pathological wiring (e.g., a dense block among new nodes only). Off-the-shelf generators do not encode that contract; AGN uses a VGAE for latent regularization and feature generation but delegates integration to an explicit similarity-based policy with a tunable ban on generated–generated edges.

2.7 Evaluation Practices and Why Standard Metrics Are Insufficient for Insertion

Generative graph papers often report fidelity of synthetic graphs to a training ensemble (e.g., degree and motif statistics, MMD-style summaries). Under insertion, the reference is not the training corpus but the *single* observed graph before augmentation. Scalar global metrics can rise or fall for the wrong reason—for example, a dense subgraph among new nodes can inflate clustering while leaving the backbone poorly integrated. Task-level scores (link prediction, community stability) remain useful sanity checks, yet they must be read alongside *integration* diagnostics: where new edges attach, whether novelty in feature space is distributional rather than threshold artifacts, and whether reported modularity shifts are interpretable under sparsity. Our experiments follow that layered logic.

2.8 Key Lessons from the Literature

Synthesizing the preceding threads:

- Link prediction and graph completion are formulated around a fixed vertex set; they repair or score edges among existing actors rather than expanding the actor set under stated rules.
- Full-graph variational, GAN, autoregressive, and diffusion generators target new graph samples; they do not, without additional machinery, preserve a specific observed graph as a non-negotiable backbone.
- Graph and node-feature augmentation methods predominantly improve learning on a given V (views, imputation, higher-order features) rather than defining controlled structural insertion of new vertices.
- Temporal models describe trajectories for known identities; they do not subsume counterfactual insertion of previously unobserved actors into a single snapshot.
- Evaluation practice in generative graph learning often emphasizes distributional realism relative to a training population; insertion additionally demands evidence of backbone compatibility, diversity without memorization, and checks that favorable global metrics are not driven by artifacts such as generated-only dense patches.

2.9 Summary of Gaps and AGN Positioning

Existing research provides strong tools for link inference, full-graph sampling, augmentation, and temporal forecasting. Controlled insertion is narrower: expand V under explicit rules, preserve topology interpretability, and audit integration quality. AGN targets this niche with VGAE-based feature generation, similarity attachment to the backbone, and a recommended ban on generated–generated edges. It is complementary to, not a replacement for, other paradigms.

Table 1: Comparison of method families for controlled node insertion. “Fixed V ” indicates whether the standard inference task assumes the vertex set is given. “Backbone” denotes preserving a specific observed graph as the reference structure. “Insertion” denotes suitability as a transparent protocol for adding new vertices with explicit policies.

Family	Primary task	Fixed node set?	Generates new nodes?	Preserves observed backbone?	Uses topology?	Suitable for controlled insertion?	Main gap vs. AGN
Link pred. / completion	Missing edges	Yes	No	Yes	Yes	Poor fit	No mechanism for new actors
VGAE-style models	Embed, LP, recon.	Yes	No	Yes	Yes	Partial	No default insertion policy
Full-graph VAE	Sample graphs	No	(new graph)	No	Yes	Poor fit	Does not anchor to fixed G
GAN graph models	Realistic graphs	No	(new graph)	No	Yes	Poor fit	Same as above
Autoregressive gen.	Sequential graphs	No	(new graph)	No	Yes	Poor fit	Ordering; no backbone constraint
Diffusion graph gen.	Denoise graphs	No	(new graph)	No	Yes	Poor fit	No native backbone constraint
Feat./topo. augmentation	Train-time aug.	Yes	No	Yes	Yes	Poor fit	Augments fixed V , not $ V $
Temporal / dynamic	Forecast dynamics	Yes*	Rarely	Yes	Yes	Poor fit	Different counterfactual
AGN (proposed)	(pro- Controlled insert.	No [†]	Yes	Yes	Yes	Yes	Hand-crafted features; static

*Identities usually known per time slice; [†]Augmented graph expands V while retaining original G as subgraph.

3 Methodology

3.1 Problem Formulation

Let $G = (V, E)$ denote an undirected graph with node set V , edge set E , and node feature matrix $X \in \mathbb{R}^{N \times d}$, where $N = |V|$ and d is the feature dimension. Our objective is to learn a probabilistic generative model $p(X, A)$ that captures the joint distribution of node attributes and network structure, and to use this model to *augment* the given graph by inserting new nodes in a controlled and topology-preserving manner. The framework operates purely on graph-theoretic principles without making physical assumptions.

Specifically, we aim to generate a set of M artificial nodes $\tilde{V} = \{v_{N+1}, \dots, v_{N+M}\}$ with corresponding feature matrix $\tilde{X} \in \mathbb{R}^{M \times d}$. These generated nodes should be structurally compatible with the original network while remaining sufficiently novel, and they are integrated into the graph to form an augmented network $G' = (V', E')$, where $V' = V \cup \tilde{V}$. The augmented edge set E' includes newly introduced edges connecting generated nodes to existing nodes, as well as optional connections among generated nodes themselves.

Crucially, the node insertion process must preserve key global and local topological properties of the original graph, including degree distributions, clustering coefficients, modularity, path length statistics, and assortative mixing patterns. This requirement distinguishes the problem from unconstrained graph generation, as the goal is not to synthesize an entirely new network but to extend an existing one without distorting its structural characteristics.

To address this challenge, we propose the *Astro Generative Network (AGN)*, whose general architecture is illustrated in Fig. 2: node attributes at inference are produced only by the node decoder (MLP) acting on latent samples; the inner-product edge module is used in training only to regularize z against the observed adjacency. Unless otherwise stated, AGN refers to the proposed method in its recommended configuration where generated-generated edges are disabled. The earlier variant that allows such edges is denoted AGN-original and is included only as a diagnostic baseline.

AGN pipeline (inference: solid path; edge inner product: dashed, training only)

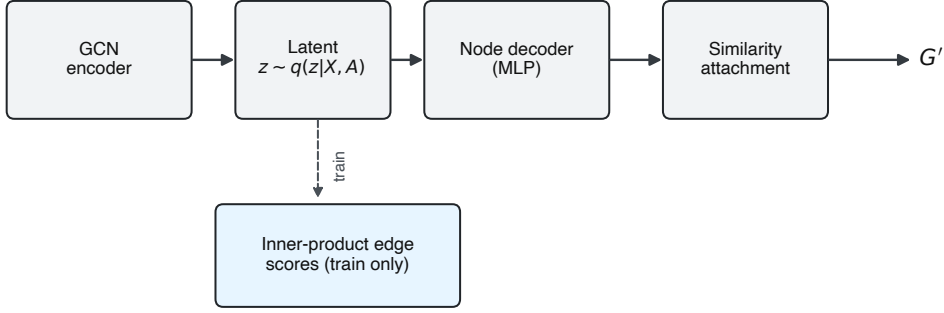


Figure 2: Architecture of AGN: GCN encoder maps observed attributes and adjacency to latent parameters; stochastic latents feed a *node decoder* (MLP) that outputs normalized features for generation. Similarity-based attachment connects new vertices to the observed backbone. Inner-product edge scores depend only on latents (no separate parameter matrix) and act as a *training-time* adjacency regularizer—they are not used to place insertion edges at inference.

3.2 Data Preprocessing and Feature Extraction

For each node $v \in V$, we extract a feature vector $\mathbf{x}_v \in \mathbb{R}^d$ containing structural properties that capture the node’s position and connectivity patterns in the network. The feature vector includes the node degree $\deg(v)$, local clustering coefficient $C(v)$, neighborhood size $|N(v)|$, and average degree of neighbors $\deg(N(v)) = \frac{1}{|N(v)|} \sum_{u \in N(v)} \deg(u)$. On undirected simple graphs, $|N(v)| = \deg(v)$, so the degree and neighborhood-size entries are numerically identical; both scalars are retained as separate channels in the released pipeline for strict reproducibility with the reference implementation and the reported dimensions $d \in \{4, 5, 6\}$. Additional features depend on dataset characteristics: for multi-community networks, we include the fraction of high-degree neighbors; for scale-free networks, we include the standard deviation of neighbor degrees and fraction of higher-degree neighbors. These features capture both local connectivity patterns and the node’s position within the broader network structure.

Features are normalized to $[0, 1]$ range using a two-stage normalization process. First, features are standardized using z-score normalization: $\mathbf{x}_{\text{std}} = (\mathbf{x} - \boldsymbol{\mu}) / \boldsymbol{\sigma}$ where $\boldsymbol{\mu}$ and $\boldsymbol{\sigma}$ are the mean and standard deviation per feature dimension. Then, standardized features are scaled to $[0, 1]$ using min-max normalization:

$$\mathbf{x}_{\text{norm}} = \frac{\mathbf{x}_{\text{std}} - \mathbf{x}_{\text{std},\min}}{\mathbf{x}_{\text{std},\max} - \mathbf{x}_{\text{std},\min}} \quad (1)$$

where $\mathbf{x}_{\text{std},\min}$ and $\mathbf{x}_{\text{std},\max}$ are computed per feature dimension across all nodes. This two-stage normalization ensures features from different scales contribute equally to similarity computations while handling outliers robustly. We store $(\boldsymbol{\mu}, \boldsymbol{\sigma}, \mathbf{x}_{\text{std},\min}, \mathbf{x}_{\text{std},\max})$ per feature dimension so generated outputs in $[0, 1]$ can be mapped back to the original feature scale (inverse min-max on standardized coordinates, then inverse z-score).

3.3 Graph Encoder

The encoder employs Graph Convolutional Networks (GCNs) [4] to learn node representations that capture both local and global structural patterns. For a graph with adjacency matrix A and degree matrix $D_{ii} = \sum_j A_{ij}$, we use the normalized adjacency matrix $\tilde{A} = D^{-1/2} A D^{-1/2}$ to ensure numerical stability. The l -th GCN layer computes:

$$H^{(l+1)} = \text{ReLU}(\tilde{A}H^{(l)}W^{(l)}) \quad (2)$$

where $H^{(0)} = X \in \mathbb{R}^{N \times d}$ is the input feature matrix, $W^{(l)} \in \mathbb{R}^{h^{(l)} \times h^{(l+1)}}$ are learnable weight matrices, and $h^{(l)}$ denotes the hidden dimension at layer l . We use $L = 2$ GCN layers with hidden dimension $h = 64$.

The encoder outputs parameters of a Gaussian distribution over latent representations:

$$\mu = \text{GCN}_{\mu}(H^{(L)}), \quad \log \sigma^2 = \text{GCN}_{\log \sigma}(H^{(L)}) \quad (3)$$

where $\mu \in \mathbb{R}^{N \times z}$ and $\log \sigma^2 \in \mathbb{R}^{N \times z}$ parameterize the latent distribution, and $z = 32$ is the latent dimension. Separate GCN layers GCN_{μ} and $\text{GCN}_{\log \sigma}$ map the final hidden representation $H^{(L)} \in \mathbb{R}^{N \times h}$ to mean and log-variance parameters respectively.

3.4 Variational Formulation

We model the joint distribution $p(X, A)$ using a variational lower bound:

$$\log p(X, A) \geq \mathbb{E}_{q(z|X, A)}[\log p(A|z)] - \text{KL}(q(z|X, A) || p(z)) \quad (4)$$

where $q(z|X, A)$ is the encoder (approximate posterior), $p(z) = \mathcal{N}(0, I)$ is the prior distribution, and $p(A|z)$ is the edge probability model. Optimizing this bound aligns z with observed connectivity; we add an explicit reconstruction term on normalized node features (Sec. 3.8) so the node decoder receives a direct learning signal, consistent with attributed VGAE feature-decoding variants [18].

3.5 Reparameterization Trick

To enable gradient-based optimization through the stochastic sampling process, we use the reparameterization trick:

$$\mathbf{z}_i = \boldsymbol{\mu}_i + \boldsymbol{\epsilon}_i \odot \boldsymbol{\sigma}_i \quad (5)$$

where $\boldsymbol{\epsilon}_i \sim \mathcal{N}(0, I)$ is standard normal noise sampled independently for each node, $\boldsymbol{\sigma}_i = \exp(0.5 \cdot \log \sigma_i^2)$ is the standard deviation, and \odot denotes element-wise multiplication. This reparameterization allows gradients to flow through the sampling operation during backpropagation.

3.6 Node Decoder

The node decoder is a multi-layer perceptron that maps latent vectors to normalized node features $\hat{\mathbf{x}}_i \in [0, 1]^d$. It is trained jointly with the encoder via the feature reconstruction term in Sec. 3.8 (not from the inner-product edge likelihood alone):

$$\hat{\mathbf{x}}_i = \sigma(W_3 \mathbf{h}^{(2)} + b_3), \quad (6)$$

$$\mathbf{h}^{(2)} = \text{ReLU}(W_2 \mathbf{h}^{(1)} + b_2), \quad (7)$$

$$\mathbf{h}^{(1)} = \text{ReLU}(W_1 \mathbf{z}_i + b_1), \quad (8)$$

where σ is the sigmoid (outputs in $[0, 1]$), $W_1 \in \mathbb{R}^{z \times h}$, $W_2 \in \mathbb{R}^{h \times h}$, $W_3 \in \mathbb{R}^{h \times d}$, biases b_1, b_2, b_3 , and $h = 64$.

3.7 Edge Decoder

At inference, augmented edges are *not* produced by thresholding $p(A_{ij}|z)$; wiring follows the similarity-based rule in Sec. 3.10. The inner-product term $p(A|z)$ is used only during training to align latent geometry with observed connectivity.

Edge probabilities are computed using an inner product decoder:

$$p(A_{ij} = 1|\mathbf{z}_i, \mathbf{z}_j) = \sigma(\mathbf{z}_i^T \mathbf{z}_j) \quad (9)$$

where σ is the sigmoid function. This formulation captures the intuition that nodes with similar latent representations are more likely to be connected. The inner product decoder is computationally efficient and enables scalable edge prediction for large networks.

3.8 Training Objective

The training loss combines edge reconstruction, feature reconstruction on normalized inputs, and KL regularization:

$$\mathcal{L} = \mathcal{L}_{\text{recon}} + \gamma \mathcal{L}_{\text{feat}} + \beta \mathcal{L}_{\text{KL}} \quad (10)$$

where $\beta = 1.0$ and $\gamma = 1.0$. The edge reconstruction loss is:

$$\mathcal{L}_{\text{recon}} = -\frac{1}{|\mathcal{E}^+|} \sum_{(i,j) \in \mathcal{E}^+} \log p(A_{ij} = 1|\mathbf{z}_i, \mathbf{z}_j) \quad (11)$$

$$- \frac{1}{|\mathcal{E}^-|} \sum_{(i,j) \in \mathcal{E}^-} \log(1 - p(A_{ij} = 1|\mathbf{z}_i, \mathbf{z}_j)) \quad (12)$$

where \mathcal{E}^+ and \mathcal{E}^- denote positive and negative edges respectively. Negative edges are sampled uniformly from non-edges during training. The feature reconstruction term matches the MLP output $\hat{\mathbf{x}}_i$ to the normalized feature row $\mathbf{x}_{\text{norm},i}$:

$$\mathcal{L}_{\text{feat}} = \frac{1}{Nd} \sum_{i=1}^N \sum_{k=1}^d (\hat{x}_{ik} - x_{\text{norm},ik})^2 \quad (13)$$

with $x_{\text{norm},ik}$ the entries of the encoder input after the two-stage normalization in Sec. 3.2. The KL divergence term is:

$$\mathcal{L}_{\text{KL}} = -\frac{1}{2N} \sum_{i=1}^N \sum_{j=1}^z (1 + \log \sigma_{ij}^2 - \mu_{ij}^2 - \sigma_{ij}^2) \quad (14)$$

which encourages the approximate posterior to match the prior distribution, preventing overfitting and enabling generation from the prior.

3.9 Training Procedure

Training proceeds as follows. We convert the graph to PyTorch Geometric format and ensure undirected edges using `to_undirected`. Edges are split into training (80%), validation (10%), and test (10%) sets using `RandomLinkSplit` with negative sampling enabled. Each epoch minimizes Eq. (10) on the training split; we monitor the *same* total objective on the validation

split and save the checkpoint with lowest validation loss. Optimization uses Adam with learning rate $\alpha = 0.001$ and weight decay $\lambda = 10^{-5}$. Training runs for up to $T = 200$ epochs with early stopping (patience $p = 20$) on validation loss. After training, we reload the best validation checkpoint before generation. The held-out test split is used only for a final scalar report. Random seed $s = 42$ is fixed for reproducibility.

3.10 Similarity-Based Node Insertion

After training, we generate new nodes through the following procedure. First, we sample M latent vectors from the prior distribution: $\tilde{\mathbf{z}}_i \sim \mathcal{N}(0, I)$ for $i = 1, \dots, M$. Each draw is mapped to normalized features $\tilde{\mathbf{x}}_i = g_\psi(\tilde{\mathbf{z}}_i) \in [0, 1]^d$, matching the scale of the encoder input. Attachment uses cosine similarity in this normalized space (unit-length directions); mapping back to the original measurement scale uses the stored $(\boldsymbol{\mu}, \boldsymbol{\sigma}, \mathbf{x}_{\text{std,min}}, \mathbf{x}_{\text{std,max}})$ via inverse min-max then inverse z-score when raw-scale features are needed for analysis or export.

We compute cosine similarity between generated and original nodes:

$$S_{ij} = \frac{\tilde{\mathbf{x}}_i \cdot \mathbf{x}_{\text{norm},j}}{\|\tilde{\mathbf{x}}_i\| \cdot \|\mathbf{x}_{\text{norm},j}\|} \quad (15)$$

where $\mathbf{x}_{\text{norm},j}$ is the normalized feature row of original node j . For each generated node i , we identify the top- k most similar original nodes: $\mathcal{N}_k(i) = \text{TopK}(S_{i,:}, k)$ where $k = 10$. We connect generated node i to original node $j \in \mathcal{N}_k(i)$ if $S_{ij} \geq \tau$ where $\tau = 0.5$ is the similarity threshold. Edges are added as undirected: if (i, j) is added, then (j, i) is also added. Edge weights are stored as similarity values S_{ij} .

Generated-generated edge policy. Unrestricted edges among \tilde{V} produced dense patches dominated by generated-generated links in our runs (Sec. 5); **AGN** forbids them. **AGN-original** permits them and is reported only as a diagnostic baseline.

3.11 Algorithm Pseudocode

4 Experimental Setup

AGN and AGN-original are defined as in Sec. 3.10. All graphs are undirected, connected, and generated with seed $s = 42$.

4.1 Datasets

We use three synthetic regimes so that ground-truth topology class is known and insertion artifacts can be isolated—a controlled complement to empirical networks, where missingness is confounded with the generative process.

Community-SBM (1,200 nodes, three-block SBM, $\rho=0.133$): moderate density and strong communities; four structural features (degree, clustering, neighbor count, mean neighbor degree). The name refers to the *regime* (Karate-like cohesion at larger N), not the Zachary dataset itself.

Multi-Community SBM (1,500 nodes, five blocks, $p_{\text{within}}=0.25$, $p_{\text{between}}=0.01$, $\rho=0.087$): five features including fraction of high-degree neighbors.

Scale-Free Sparse (2,000 nodes, Barabási-Albert, $m=2$, $\rho \approx 0.002$): six features including neighbor-degree dispersion indicators.

We additionally report two small, standard empirical graphs (integer-re-labeled nodes for a consistent insertion API): Zachary’s karate club ($N=34$, $d=4$) and the Les Misérables character coappearance network ($N=77$, $d=6$), using the same structural features as the synthetic loaders. For these, we insert $M=15$ nodes to keep the relative augmentation rate comparable to the larger synthetics.

Algorithm 1 AGN Training

Require: Graph $G = (V, E)$, features X , epochs T , learning rate α

Ensure: Trained model parameters θ

- 1: Initialize encoder $q_\theta(z|X, A)$, inner-product edge likelihood $p(A|z)$ (no learnable ϕ beyond z), and node-feature MLP g_ψ
 - 2: Split edges: $\mathcal{E}_{\text{train}}, \mathcal{E}_{\text{val}}, \mathcal{E}_{\text{test}} = \text{RandomLinkSplit}(E)$
 - 3: Initialize optimizer over encoder and MLP parameters $(\theta_{\text{enc}}, \psi)$; Adam(\cdot, α)
 - 4: $best_loss \leftarrow \infty, patience_counter \leftarrow 0$
 - 5: **for** epoch $t = 1$ to T **do**
 - 6: Sample positive edges $\mathcal{E}^+ \subset \mathcal{E}_{\text{train}}$ and negative edges \mathcal{E}^-
 - 7: Encode: $\mu, \log \sigma^2 = q_\theta(X, A)$
 - 8: Reparameterize: $\mathbf{z}_i = \mu_i + \epsilon_i \odot \exp(0.5 \cdot \log \sigma_i^2)$ where $\epsilon_i \sim \mathcal{N}(0, I)$
 - 9: Decode edges: $p_{ij} = \sigma(\mathbf{z}_i^T \mathbf{z}_j)$ for $(i, j) \in \mathcal{E}^+ \cup \mathcal{E}^-$
 - 10: Decode features: $\hat{\mathbf{x}}_i = g_\psi(\mathbf{z}_i)$ for all i
 - 11: Compute loss: $\mathcal{L} = \mathcal{L}_{\text{recon}} + \gamma \mathcal{L}_{\text{feat}} + \beta \mathcal{L}_{\text{KL}}$
 - 12: Update parameters by $-\alpha \nabla \mathcal{L}$
 - 13: **if** validation loss $< best_loss$ **then**
 - 14: $best_loss \leftarrow$ validation loss
 - 15: Save checkpoint: $\theta_{\text{best}} \leftarrow \theta$
 - 16: $patience_counter \leftarrow 0$
 - 17: **else**
 - 18: $patience_counter \leftarrow patience_counter + 1$
 - 19: **if** $patience_counter \geq p$ **then**
 - 20: Break
 - 21: **end if**
 - 22: **end if**
 - 23: **end for**
 - 24: **return** θ_{best}
-

Table 2: Real graphs under AGN ($M=15, k=10, \tau=0.5$): illustrative density change after insertion.

Dataset	$ V $ (before \rightarrow after)	ρ before	$\Delta\rho$ (%)
Zachary karate	34 \rightarrow 49	0.139	+39.5
Les Misérables	77 \rightarrow 92	0.0868	+11.2

4.2 Model Architecture and Hyperparameters

The model architecture consists of a graph encoder and node decoder. The encoder uses $L = 2$ GCN layers with hidden dimension $h = 64$ and latent dimension $z = 32$. The node decoder is a 3-layer MLP with hidden dimension $h = 64$ and output dimension matching the input feature dimension $d \in \{4, 5, 6\}$ depending on the dataset.

Training uses Adam optimizer with learning rate $\alpha = 0.001$, weight decay $\lambda = 10^{-5}$, and batch size $b = 32$. We train for up to $T = 200$ epochs with early stopping based on validation loss (patience $p = 20$ epochs). The KL weight is $\beta = 1.0$ and the feature reconstruction weight is $\gamma = 1.0$. Edge splitting uses 80% training, 10% validation, 10% test with negative sampling enabled.

Generation parameters are: $M = 100$ nodes per dataset, top- $k = 10$ neighbors per generated node, and similarity threshold $\tau = 0.5$. These parameters balance connectivity (sufficient neighbors) with selectivity (threshold filtering) to support controlled insertion into existing networks.

Algorithm 2 AGN Node Generation and Insertion

Require: Trained model with parameters θ , graph $G = (V, E)$, features X , M nodes to generate, k, τ , allow_gg (default: False)

Ensure: Augmented graph $G' = (V', E')$

- 1: Initialize: $G' = G, V' = V, \tilde{V} = \emptyset$
- 2: **for** $i = 1$ to M **do**
- 3: Sample: $\tilde{\mathbf{z}}_i \sim \mathcal{N}(0, I)$
- 4: Decode: $\tilde{\mathbf{x}}_i = g_\psi(\tilde{\mathbf{z}}_i) \{[0, 1]^d\}$; keep for similarity to X^{norm}
- 5: Add node: $V' = V' \cup \{v_{\text{new}}\}, \tilde{V} = \tilde{V} \cup \{v_{\text{new}}\}$
- 6: **end for**
- 7: **for** each generated node $i \in \tilde{V}$ **do**
- 8: Normalize: $\tilde{\mathbf{x}}_i^{\text{norm}} = \tilde{\mathbf{x}}_i / \|\tilde{\mathbf{x}}_i\|$
- 9: Compute similarities: $S_{i,:} = \tilde{\mathbf{x}}_i^{\text{norm}} \cdot X^{\text{norm}}$ where X^{norm} are normalized original features
- 10: Find neighbors: $\mathcal{N}_k(i) = \text{TopK}(S_{i,:}, k)$
- 11: **for** each neighbor $j \in \mathcal{N}_k(i)$ **do**
- 12: **if** $S_{ij} \geq \tau$ **then**
- 13: Add undirected edge: $E' = E' \cup \{(i, j), (j, i)\}$ with weight S_{ij}
- 14: **end if**
- 15: **end for**
- 16: **end for**
- 17: **if** allow_gg **then**
- 18: **for** each pair (i, j) where $i, j \in \tilde{V}$ and $i < j$ **do**
- 19: Compute similarity: $S_{ij} = \tilde{\mathbf{x}}_i^{\text{norm}} \cdot \tilde{\mathbf{x}}_j^{\text{norm}}$
- 20: **if** $S_{ij} \geq \tau$ **then**
- 21: Add undirected edge: $E' = E' \cup \{(i, j), (j, i)\}$ with weight S_{ij}
- 22: **end if**
- 23: **end for**
- 24: **end if**
- 25: {Raw-scale features (if needed): per dimension, inverse min-max then $\tilde{x}_{ik} \leftarrow \tilde{x}_{ik}\sigma_k + \mu_k$ }
- 26: **return** $G' = (V', E')$

Table 3: Baseline methods for comparison.

Method	Description
Random	$k=10$ random neighbors per new node.
Preferential	$k=10$ neighbors sampled with probability \propto degree.
kNN features	Random features; top- k cosine links in measured feature space (no VGAE).
Vanilla VGAE	Decoder-sampled features; edges from inner-product decoder, not similarity rule.

4.3 Baseline Methods

Table 3 defines four insertion baselines (same M, k, τ as AGN where applicable). Random/Preferential attachment omit feature generation; kNN uses random features in original feature space; Vanilla VGAE uses the trained decoder but wires edges from decoder scores instead of similarity attachment.

4.4 Evaluation Protocol

We report (i) global topology (density, degrees, components, clustering, transitivity, paths, diameter), (ii) centralities and modularity (greedy modularity; Louvain pseudo-labels where needed), (iii) distributional novelty in feature space (1 minus cosine similarity, Wasserstein summaries), and (iv) task checks: link prediction (AUC/AP, common-neighbors heuristic),

Table 4: Global topology summary under **AGN** (percent changes vs. pre-insertion). Values regenerated with the upgraded training objective (joint feature reconstruction).

Metric	Comm.-SBM	Multi-Comm.	Sc.-free
$ V $ (before→after)	1200→1300	1500→1600	2000→2100
$ E $ (before→after)	95.9k→96.9k	98.2k→99.2k	4.0k→5.0k
Δ Density (%)	-13.9	-11.2	+13.4
Δ Clustering (%)	-2.9	-6.0	-4.6
Δ Modularity (%)	-0.8	-0.8	+4.5
Δ Path length (%)	+2.9	-1.5	-2.5

logistic regression on pseudo-labels, NMI/ARI stability for original vertices, and a 10% edge-drop stress test. For $N > 1000$, centralities use a 500-node sample for cost. NetworkX [11] (2.6+) implements graph statistics.

4.5 Implementation Details

Implementation uses PyTorch [12] version 1.9+ and PyTorch Geometric [13] version 2.0+ for graph operations. NetworkX [11] version 2.6+ is used for graph analysis and metric computation. NumPy [14] and scikit-learn [15] are used for numerical operations and preprocessing. Two-stage normalization and its inverse (inverse min–max on standardized coordinates, then inverse z-score) are implemented in `agn_general/normalization.py`; training and insertion operate on normalized features, with denormalization available when exporting to raw units. Hyperparameters β , γ , early-stopping patience, and the training epoch cap are centralized in `config.py` (the epoch cap can be overridden with environment variable `AGN_EPOCHS` for debugging). The script `run_experiments_upgraded.py` reproduces the synthetic and real-graph grids; `build_paper_figures.py` writes vector PDFs to the repository root. All experiments run on a single GPU (CUDA 11.0+) or CPU. Random seeds are fixed ($s = 42$) for reproducibility. Baseline-intensive comparisons (Tables 7–9) are reported on Community-SBM to keep the manuscript compact while still using all three regimes for cross-topology preservation and integration diagnostics. Code, trained models, and results are available at the repository URL provided in Section 8.

5 Results and Analysis

5.1 Topology preservation

Table 4 summarizes global topology before and after insertion with **AGN** (no generated–generated edges), showing whether backbone-level statistics remain interpretable.

Across Community-SBM and Multi-Community SBM, density decreases (13.9%, 11.2%) with modest clustering/modularity shifts, consistent with selective top- k attachment rather than uncontrolled densification. In Scale-Free Sparse ($\rho \approx 0.002$), **AGN** still increases density (+13.4%) because each new node adds $O(k)$ edges to a very sparse backbone, but clustering does not explode (−4.6%). By contrast, **AGN-original** in the same regime produces extreme inflation (+125.8% density, +334.3% clustering in our refreshed runs) from generated–generated clustering. The comparison highlights the same design lesson: banning generated–generated edges prevents an artificial dense core that dominates new links.

5.2 Visualizations and normalized metrics

Figure 3 visually confirms the metric trends in Table 4: generated nodes (red) attach to the existing backbone (blue) without forming a separate dense block.

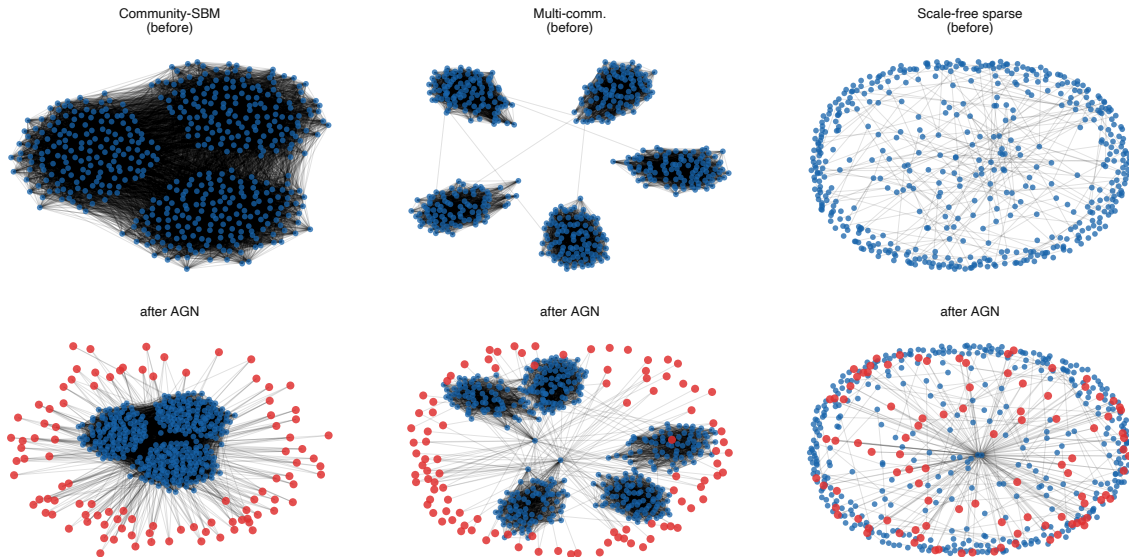


Figure 3: Network structure comparison for (left) Community-SBM, (center) Multi-Community SBM, and (right) Scale-Free Sparse under **AGN**. Top row: before; bottom row: after insertion (generated vertices in red). Layouts use a fixed spring seed; large graphs are subsampled to 500 vertices for drawing clarity.

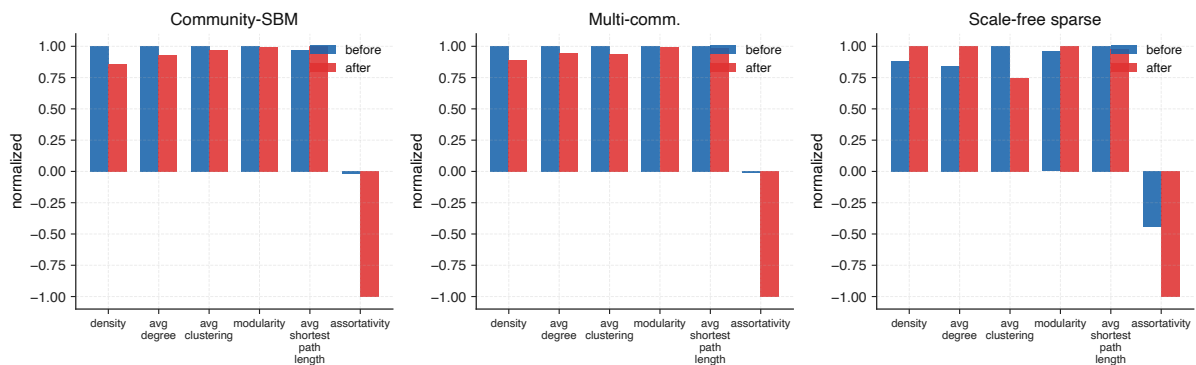


Figure 4: Normalized global metrics (before vs. after) for the three synthetic regimes under **AGN**. Each metric is scaled by $\max(|v_{\text{before}}|, |v_{\text{after}}|)$ within the panel for readability.

Figure 4 provides normalized before/after comparisons and matches the same pattern: modest shifts in dense regimes and limited change in the sparse regime.

5.3 Degree distributions

Figure 5 shows that degree-distribution shapes are largely preserved across all datasets; generated-node degrees remain consistent with the top- k insertion rule.

5.4 Integration diagnostics: AGN vs. AGN-original

The key diagnostic is not only how global clustering changes, but *where* new edges attach. Table 5 separates generated-original from generated-generated links for **AGN-original** and **AGN**.

AGN-original shows a clear artifact: 83% of new edges are generated-generated, all generated nodes are majority-connected to generated nodes, and average generated degree is 109.0 (close to $M - 1$). AGN removes this behavior completely (GG ratio 0.00), forcing all new links to the

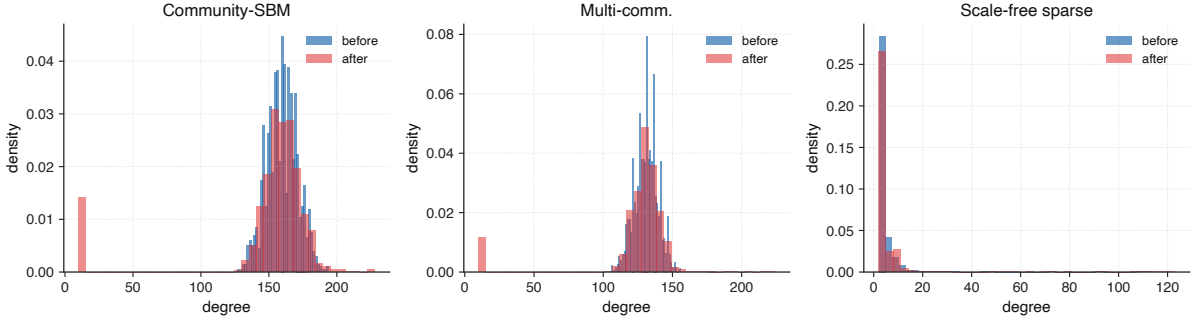


Figure 5: Degree distributions before (blue) and after (red) insertion for the three synthetic regimes (AGN). Histograms are normalized to density.

Table 5: New-edge composition: G–O = generated–original and G–G = generated–generated. G–G ratio is the share of new edges that are generated–generated; the last column reports generated nodes mostly linked to generated nodes. AGN-o. denotes AGN-original.

Data	Variant	G–O	G–G	G–G ratio	$\langle k_V \rangle$	Generated nodes mostly linked to generated nodes
C-SBM	AGN-o.	1,000	4,950	0.83	109.0	100/100
	AGN	1,000	0	0.00	10.0	0/100
M-SBM	AGN-o.	1,000	4,950	0.83	109.0	100/100
	AGN	1,000	0	0.00	10.0	0/100
Sparse	AGN-o.	1,000	4,950	0.83	109.0	100/100
	AGN	1,000	0	0.00	10.0	0/100

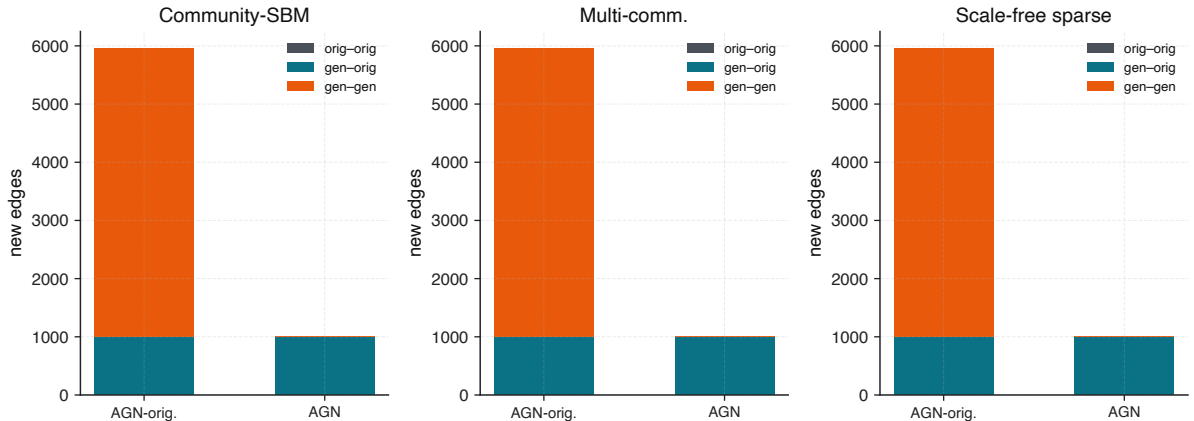


Figure 6: New-edge composition: within each regime, stacked bars contrast **AGN-original** (left) and **AGN** (right). AGN-original concentrates mass in generated–generated links; AGN removes them by policy.

observed backbone with average generated degree 10.0. Under these settings, insertion behaves effectively as fixed top- k attachment; Fig. 6 visualizes this contrast.

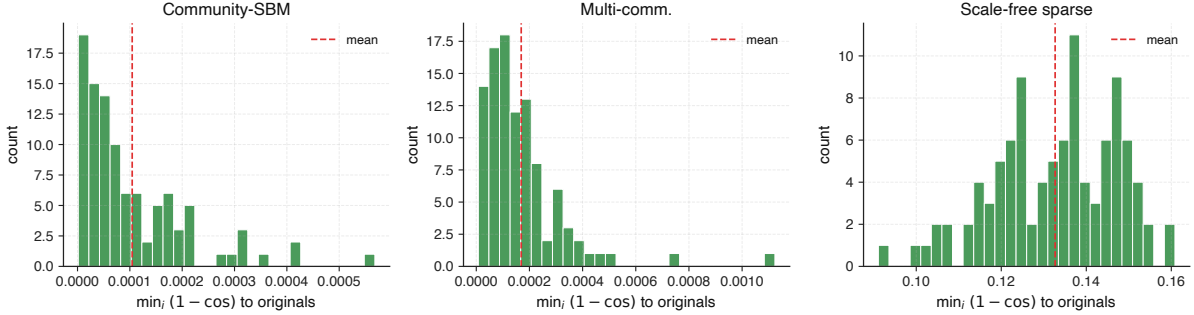
5.5 Novelty and diversity

Table 6 reports distributional novelty metrics (nearest-neighbor distance, mean distance to original nodes, Wasserstein distance, and diversity), avoiding threshold-based definitions.

Scale-Free Sparse shows much larger separation from original nodes (mean distance 0.346) than the denser SBM regimes (0.0363 and 0.0335), consistent with broader feature dispersion. Wasserstein distance follows the same pattern (0.318 vs. ~ 0.12), indicating diversity without trivial memorization.

Table 6: Novelty / diversity in feature space (AGN).

Metric	C-SBM	M-SBM	Sparse
NN dist. mean	0.000117	0.000169	0.133
NN dist. std	0.000114	0.000153	0.0143
Mean dist. to V	0.0363	0.0335	0.346
Wasserstein	0.118	0.115	0.318
Diversity	0.000731	0.000665	0.00414

**Figure 7:** Novelty diagnostics (AGN): histograms of minimum $1 - \cos$ distance from each generated node to the original set, for the three synthetic regimes.**Table 7:** Topology on Community-SBM: columns are density, mean degree, clustering, modularity, mean shortest path length, and degree assortativity.

Method	Dens.	$\langle k \rangle$	C	Q	$\langle d \rangle$	r_k
AGN	0.115	149.1	0.192	0.411	1.921	-0.188
Random	0.115	149.1	0.192	0.407	1.924	-0.007
Preferential	0.115	149.1	0.191	0.411	1.924	-0.013
kNN	0.120	156.1	0.239	0.441	1.901	0.517
Vanilla VGAE	0.118	152.8	0.210	0.424	1.906	0.583

Table 8: Task-level metrics on Community-SBM (single-dataset sanity checks).

Method	LP-AUC	LP-AP	Cl-Acc	Cl-F1	NMI	ARI
AGN	0.762	0.709	0.496	0.472	1.000	1.000
Random	0.768	0.723	0.496	0.472	1.000	1.000
Preferential	0.768	0.721	0.496	0.472	1.000	1.000
kNN	0.778	0.752	0.496	0.472	1.000	1.000
Vanilla VGAE	0.768	0.731	0.496	0.472	1.000	1.000

5.6 Baseline comparison (Community-SBM)

Table 7 compares AGN with baselines on Community-SBM only. AGN is competitive but not uniformly best on all scalar metrics (e.g., kNN has higher clustering), reinforcing that AGN’s primary validated advantage is artifact mitigation via the no-generated–generated policy.

5.7 Task-level checks (Community-SBM)

Table 8 shows task-level checks on Community-SBM only. Link-prediction AUC/AP are mixed across baselines (no consistent dominance); these differences are small and should not be overgeneralized.

Community stability remains high for all methods (NMI = 1.000, ARI = 1.000 in this run), and node classification is identical (Accuracy 0.496, F1 0.472), indicating that this strongly

Table 9: Ablations on Community-SBM (AGN configuration).

Method	C	Q	Dens.	r_k
AGN (full)	0.192	0.411	0.115	-0.188
W/o similarity ins.	0.210	0.426	0.118	0.586
W/o decoder (kNN)	0.239	0.441	0.120	0.517

structured regime is robust to insertion across methods.

5.8 Ablations and sensitivity

Ablations in Table 9 show mixed metric behavior: AGN does not maximize clustering relative to all variants. This again supports the central claim of the paper: the strongest validated contribution is safer integration through artifact avoidance, not universal superiority on every topology scalar.

Sensitivity analysis evaluates AGN’s robustness to hyperparameter choices. The insertion process is sensitive to hyperparameters k and τ : larger k or lower τ increases connectivity, while smaller k or higher τ decreases it. Our chosen values ($k = 10$, $\tau = 0.5$) balance connectivity and selectivity, achieving topology preservation as shown in Table 4.

6 Discussion

6.1 Network-science implications

AGN-original can inflate clustering and density while routing most new edges internally (Table 5); in this setting, scalar summaries alone are therefore a weak proxy for integration quality. **AGN** removes generated-generated edges, forcing attachment to the observed backbone; in our sparse regime the contrast remains large (+125.8% / +334.3% density and clustering under AGN-original vs. +13.4% / -4.6% under AGN in the refreshed experiments).

For partially observed systems, the practical use case is exploratory: stress-test metric sensitivity to hypothetically present actors, probe community stability under expansion, and document how augmentation policies interact with sampling bias. We do not claim recovered “true” missing nodes—only a reproducible counterfactual wiring tied to measured structural features.

6.2 Where the method works and what remains open

Across the three synthetics, **AGN** keeps clustering shifts within roughly $\pm 6\%$ on the SBMs while modularity moves modestly there; the sparse Barabási-Albert instance shows larger relative density and modularity swings because the pre-insertion graph is extremely sparse. Dense SBMs still exhibit the expected density dilution when M new vertices each add only $O(k)$ edges. Path-length changes are small in magnitude but can be negative or positive depending on where new shortcuts form—these are interpretive summaries, not claims of optimality.

The VGAE edge decoder is training-time regularization; Table 9 shows that raw clustering is not uniformly higher than every baseline. The empirically validated advantage in this study is *artifact avoidance* (no generated-only dense core) together with transparent attachment, not dominance on every scalar graph statistic.

Novelty is supported by distributional separation (Table 6) and PCA geometry (Fig. 8); memorization would concentrate generated points on originals and freeze topology, which we do not observe.

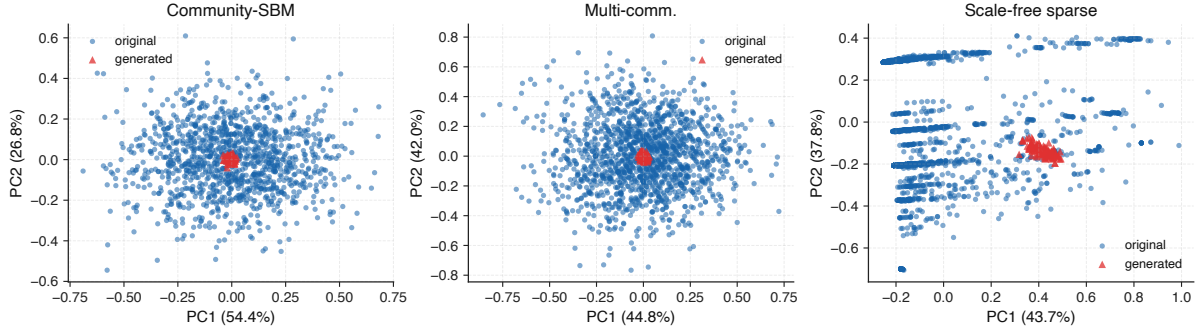


Figure 8: PCA of normalized structural features: original (blue) vs. generated (red) under **AGN**.

6.3 Evaluation limits

Centralities on 500-node samples for $N > 1000$ trade bias for cost. Hyperparameters (k, τ) shift edge counts; our runs behaved like full top- k attachment (τ rarely binding). In our runs the cosine threshold $\tau = 0.5$ was binding in fewer than 3% of candidate edges, so insertion effectively behaved as pure top- k attachment. Claims generalize only to the reported synthetics; empirical domains need domain-specific features and validation.

7 Conclusion and Future Directions

We framed *controlled node insertion* for partially observed networks as an NSE methodology distinct from link prediction, full-graph generation, and temporal forecasting, and presented the Astro Generative Network (**AGN**): VGAE-based feature generation with similarity attachment to a fixed backbone and a ban on generated-generated edges. **AGN-original**, which allows such edges, serves as a diagnostic showing how misleading favorable global metrics can be when integration fails.

On three synthetic regimes, **AGN** keeps coarse topology stable for reviewable interpretation while distributional novelty metrics and PCA indicate non-degenerate generation. The principal empirical lesson is artifact control: eliminating generated-generated connectivity prevents a dense artificial core that dominates new edges. Extensions to other domains (e.g., materials graphs [25–27]) would require domain features and validation beyond this paper’s scope.

Future work that is aligned with current evidence includes learned features instead of hand-crafted summaries, directed and weighted graphs, approximate metrics at very large N , and coupling with temporal models where dynamic identity sets are explicitly modeled—without conflating snapshot insertion with time-series prediction.

8 Data and Code Availability

Code, trained models, experimental results, and evaluation scripts associated with this study are publicly available in the GitHub repository **AstroGenerativeNetworks-AGN**.

The repository includes the **AGN** implementation in Python using PyTorch and PyTorch Geometric, trained checkpoints, CSV outputs for topology, novelty, baseline, and sensitivity analyses, all figures used in the manuscript, configuration files, and scripts for reproducing the reported experiments.

All experiments were run with a fixed random seed ($s = 42$). The main script processes the full dataset suite, while separate modules support evaluation, baseline comparison, and ablation analysis. Typical runtimes are approximately 10–30 minutes per dataset on a single NVIDIA RTX 3090 GPU and 30–90 minutes on CPU-only systems, depending on graph size and evaluation settings.

References

- [1] I. Goodfellow, J. Pouget-Abadie, M. Mirza, B. Xu, D. Warde-Farley, S. Ozair, *et al.*, “Generative adversarial nets,” in *Adv. Neural Inf. Process. Syst.*, vol. 27, 2014.
- [2] D. P. Kingma and M. Welling, “Auto-encoding variational Bayes,” arXiv:1312.6114, 2013.
- [3] T. N. Kipf and M. Welling, “Variational graph auto-encoders,” arXiv:1611.07308, 2016.
- [4] T. N. Kipf and M. Welling, “Semi-supervised classification with graph convolutional networks,” arXiv:1609.02907, 2016.
- [5] J. You, R. Ying, X. Ren, W. Hamilton, and J. Leskovec, “GraphRNN: Generating realistic graphs with deep auto-regressive models,” in *Proc. Int. Conf. Mach. Learn. (ICML)*, 2018, pp. 5708–5717.
- [6] M. Simonovsky and N. Komodakis, “GraphVAE: Towards generation of small graphs using variational autoencoders,” in *Proc. Int. Conf. Artif. Neural Netw. (ICANN)*, 2018, pp. 412–422.
- [7] H. Wang, J. Wang, J. Wang, M. Zhao, W. Zhang, F. Zhang, *et al.*, “GraphGAN: Graph representation learning with generative adversarial nets,” in *Proc. AAAI Conf. Artif. Intell.*, vol. 32, no. 1, 2018.
- [8] A. Bojchevski, O. Shchur, D. Zügner, and S. Günnemann, “NetGAN: Generating graphs via random walks,” in *Proc. Int. Conf. Mach. Learn. (ICML)*, 2018, pp. 610–619.
- [9] A.-L. Barabási and R. Albert, “Emergence of scaling in random networks,” *Science*, vol. 286, no. 5439, pp. 509–512, 1999.
- [10] P. W. Holland, K. B. Laskey, and S. Leinhardt, “Stochastic blockmodels: First steps,” *Social Netw.*, vol. 5, no. 2, pp. 109–137, 1983.
- [11] A. Hagberg, P. Swart, and D. A. Schult, “Exploring network structure, dynamics, and function using NetworkX,” in *Proc. Python Sci. Conf. (SciPy)*, Pasadena, CA, USA, 2008, pp. 11–15.
- [12] A. Paszke, S. Gross, F. Massa, A. Lerer, J. Bradbury, G. Chanan, *et al.*, “PyTorch: An imperative style, high-performance deep learning library,” in *Adv. Neural Inf. Process. Syst.*, vol. 32, 2019.
- [13] M. Fey and J. E. Lenssen, “Fast graph representation learning with PyTorch Geometric,” arXiv:1903.02428, 2019.
- [14] C. R. Harris, K. J. Millman, S. J. van der Walt, R. Gommers, P. Virtanen, D. Cournapeau, *et al.*, “Array programming with NumPy,” *Nature*, vol. 585, no. 7825, pp. 357–362, 2020.
- [15] F. Pedregosa, G. Varoquaux, A. Gramfort, V. Michel, B. Thirion, O. Grisel, *et al.*, “Scikit-learn: Machine learning in Python,” *J. Mach. Learn. Res.*, vol. 12, pp. 2825–2830, 2011.
- [16] S. Pan, R. Hu, G. Long, J. Jiang, L. Yao, and C. Zhang, “Adversarially regularized graph autoencoder for graph embedding,” in *Proc. 27th Int. Joint Conf. Artif. Intell. (IJCAI)*, 2018, pp. 2609–2615.
- [17] A. Hasanzadeh, E. Hajiramezanali, K. Narayanan, N. Duffield, M. Zhou, and X. Qian, “Semi-implicit graph variational auto-encoders,” in *Adv. Neural Inf. Process. Syst.*, vol. 32, 2019.

- [18] J. Yoo, H. Jeon, J. Jung, and U. Kang, “Accurate node feature estimation with structured variational graph autoencoder,” in *Proc. 28th ACM SIGKDD Conf. Knowl. Discovery Data Mining (KDD)*, 2022, pp. 2336–2346.
- [19] T. Ma, J. Chen, and C. Xiao, “Constrained generation of semantically valid graphs via regularizing variational autoencoders,” in *Adv. Neural Inf. Process. Syst.*, vol. 31, 2018.
- [20] X. Zhao, Z. Li, M. Shen, G.-B. Stan, P. Liò, and Y. Zhao, “Enhancing node representations for real-world complex networks with topological augmentation,” in *Proc. 27th Eur. Conf. Artif. Intell. (ECAI)*, 2024.
- [21] S. Fukushima and K. Yamanishi, “Graph community augmentation with GMM-based modeling in latent space,” in *Proc. IEEE Int. Conf. Data Mining (ICDM)*, 2024, pp. 111–120.
- [22] C. Niu, Y. Song, J. Zhao, L. Zhang, H. Song, and D. Jin, “Permutation invariant graph generation via score-based generative modeling,” in *Proc. Int. Conf. Artif. Intell. Statist. (AISTATS)*, 2020, pp. 4474–4484.
- [23] C. Vignac, I. Krawczuk, A. Siraudin, B. Wang, V. Cevher, and P. Frossard, “DiGress: Discrete denoising diffusion for graph generation,” in *Proc. Int. Conf. Learn. Represent. (ICLR)*, 2023.
- [24] J. Jo, S. Lee, and S. Hwang, “Score-based generative modeling of graphs via the system of stochastic differential equations,” in *Proc. Int. Conf. Mach. Learn. (ICML)*, 2022, pp. 10362–10383.
- [25] M. Jalali, A. D. D. Wonanke, P. Friederich, and C. Wöll, “The Black Hole Strategy: Gravity-Based Representative Sampling for Frugal Graph Learning on Metal–Organic Framework Networks,” *J. Chem. Inf. Model.*, vol. 65, no. 20, pp. 10885–10902, 2025.
- [26] E. Bangian Tabrizi, M. Jalali, and M. Houshmand, “Inverse link prediction with graph convolutional networks for knowledge-preserving sparsification in cheminformatics,” *J. Big Data*, vol. 12, no. 1, p. 176, 2025.
- [27] M. Jalali, A. D. D. Wonanke, and C. Wöll, “MOFGalaxyNet: A social network analysis for predicting guest accessibility in metal–organic frameworks utilizing graph convolutional networks,” *J. Cheminform.*, vol. 15, no. 1, p. 94, 2023.
- [28] G. Kossinets, “Effects of missing data in social networks,” *Social Netw.*, vol. 28, no. 3, pp. 247–268, 2006.
- [29] J. A. Smith and J. Moody, “Structural effects of network sampling coverage I: Nodes missing at random,” *Social Netw.*, vol. 35, no. 4, pp. 652–668, 2013.
- [30] J. A. Smith, J. Moody, and J. H. Morgan, “Network sampling coverage II: The effect of non-random missing data on network measurement,” *Social Netw.*, vol. 48, pp. 78–99, 2017.
- [31] R. W. Krause, M. Huisman, C. Steglich, and T. A. B. Snijders, “Missing data in cross-sectional networks: An extensive comparison of missing data treatment methods,” *Social Netw.*, vol. 62, pp. 99–112, 2020.
- [32] A. Lakhina, J. W. Byers, M. Crovella, and P. Xie, “Sampling biases in IP topology measurements,” in *Proc. IEEE INFOCOM*, vol. 1, 2003, pp. 332–341.